

NEURM012 Final Report

Evaluation of Methodologies for the Identification of Head Direction Cells

**Anthony G. Chen
Affiliate Neurosciences
SN: 17152555
anthony.chen.17@ucl.ac.uk**

Word Count: 1939

Introduction and Background

Head direction (HD) cells are characterized by a preferred tuning towards a single, allocentric direction and play essential roles in spatial navigation – one of the most fundamental functions for mammalian survival [1, 2]. In order to compute the HD “tuning-curve”, a traditional approach used is to simply divide the overall spike events in a particular direction by the time spent in that direction [3].

The dataset is acquired from Peyrache, A., Buzsáki, G. (2015) and contains multi-electrode recordings made from the anterior thalamus and subiculum areas of freely moving mice during food foraging [4]. The head direction and location of the mice are also provided. The authors used the data to compare the contribution between stimulus-driven and internally-generated activities through comparison between sleep- and wake-states [5]. For my analysis, data from a single mouse from a single session is used (“Mouse12-120806”), for a total of 8 electrodes recording from the anterior thalamus (mainly the antero-dorsal nucleus) and 41 identifiable clusters / cells.

Given the traditional way of identifying HD tuning, I set out to answer the question of whether or not this method offers a good way of detecting the neuron’s “true” underlying directional preference. Concretely, I will first compute the tuning curve using the aforementioned method and test each neuron for directional selectivity, then evaluate the tuning curve via cross-validation on unseen data.

Exploratory Analysis

The spike time and cluster data from each electrode along with the head direction data are imported into *Jupyter Notebook (Python3)*. A raster plot is generated to visualize the spiking pattern of each cluster (Fig. 1B), shown alongside the recorded HD angle (Fig. 1A).

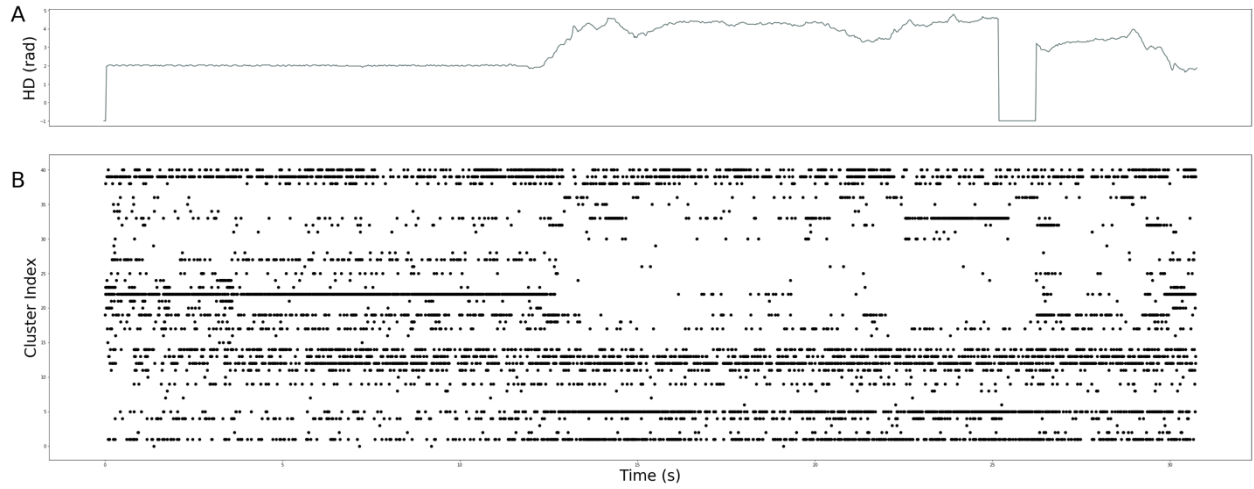


Figure 1: (A) Head direction angle of the mouse for the first ~30 seconds of the recording session. Notice that at certain points (e.g. ~25s) the head angle dips to -1 rad, this is due to poor recording quality that was not properly registered. Improperly recorded head direction data are shown here for raw data visualization, but are discarded from subsequent analysis. (B) Raster plot of showing spiking events of the 41 clusters over the first ~30s of the recording session.

Since the spikes and HD are recorded at different frequencies, each spiking time-point is down-sampled from 20,000Hz to 39.06Hz and rounded to the nearest integer to acquire the head angle at that spike. Both the spikes and the head angles are then quality-controlled via excluding improperly recorded head directions.

For each of the recorded cluster, spike and occupancy histograms are generated to indicate the head direction at which the cell spikes, and the total amount of time the mouse spent in each head direction over the length of the recording session. Both histograms are smoothed with a Gaussian kernel with a standard deviation of 6° (Fig. 2A, 2B). An averaged spiking rate for each head direction (henceforth referred to as “HD field”) is generated (Fig. 2C, 2D) via dividing the smoothed spike histogram (Fig. 2A) by the smoothed occupancy histogram (Fig. 2B).

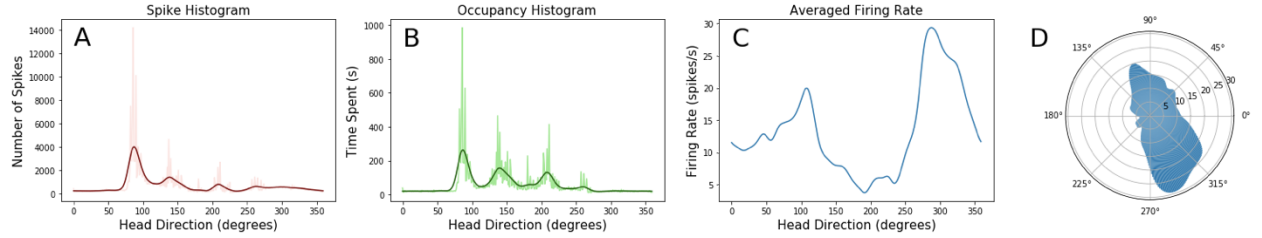


Figure 2: Steps to compute the head direction field, defined as the averaged cell firing rate at each angle. Both the spikes and occupancy are binned with a bin width of 1 degree and smoothed with a Gaussian window with a standard deviation of 6° . The light and dark colours for both the spikes (**A**) and occupancy histograms (**B**) correspond to the pre- and post-smoothed signal, respectively. The blue signal in (**C**) is the quotient of A and B, which shows the averaged firing rate of this cell at each angle (i.e. the HD field of this cluster). (**D**) Illustrates the same information as (**C**) but plotted on a polar coordinate system.

Below, the HD field of all 41 detected clusters are displayed (Fig.3). Viewed purely qualitatively, I observe a number of promising candidates for direction selectivity (e.g. index 7, 19, 33, etc.). I also expect certain cells to show no direction selectivity (e.g. index 10, 15, 40). Interestingly, certain cells show a “fan-like” firing distribution, with a wide distribution of high-firing regions, but still seemly showing a preference towards one side (E.g. index 14). Currently I can only speculate that these cells, while appearing as having a directional preference, are not actually directional sensitive. I thus hypothesized that the cross-validation method will show less cells as being directional sensitive as compared to a method that simply test for the distribution of a HD field.

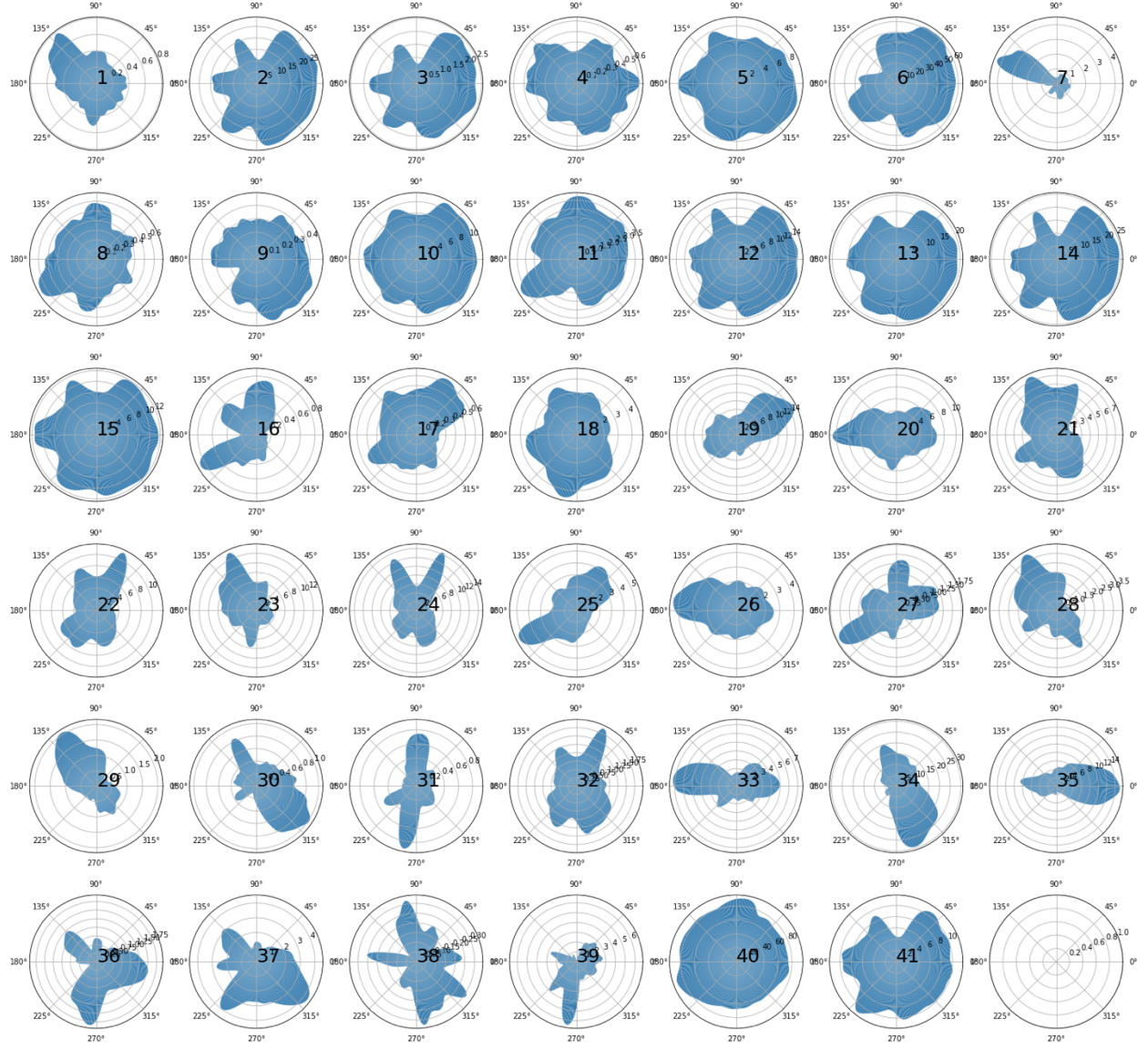


Figure 3: HD field for all detected clusters (i.e. averaged firing rate as a function of head angle), visualized on polar coordinates. The number in each polar plot are indices I have used to index different detected clusters. Note that each polar plot's radius is different to best visualize the data for that individual plot (i.e. no standard radius is used across all polar plots shown above).

Confirmatory Analysis

Sec.1: Most HD fields show dependency of firing rate on head angle

Permutation testing is used as a non-parametric way to examine the alternative hypothesis of a dependency of firing rate on head angle. The strength of the mean firing rate vector is computed for the HD field of each cell as follows, where r_i denotes a 2-D vector whose modulus is the firing rate of the cell in the i -th degree:

$$|\bar{r}| = \frac{1}{360} \left| \sum_{i=1}^{360} r_i \right|$$

The mean vector for each cell is tested against a null distribution generated by repeatedly shuffling the HD field vectors' magnitudes (for that cell) with respect to their angles, then computing the modulus of the shuffled mean vector. Concretely, the null distribution represents a distribution of the mean vector magnitude of HD fields whose firing rate do not depend on head angle.

Of the 41 clusters tested, 40 (98%) show a significant dependency of firing rate on head direction angle after Bonferroni correction with a group $\alpha = 0.05$. Fig.4 illustrates the z-score of the null distribution with the actual mean vector magnitude of the HD field.

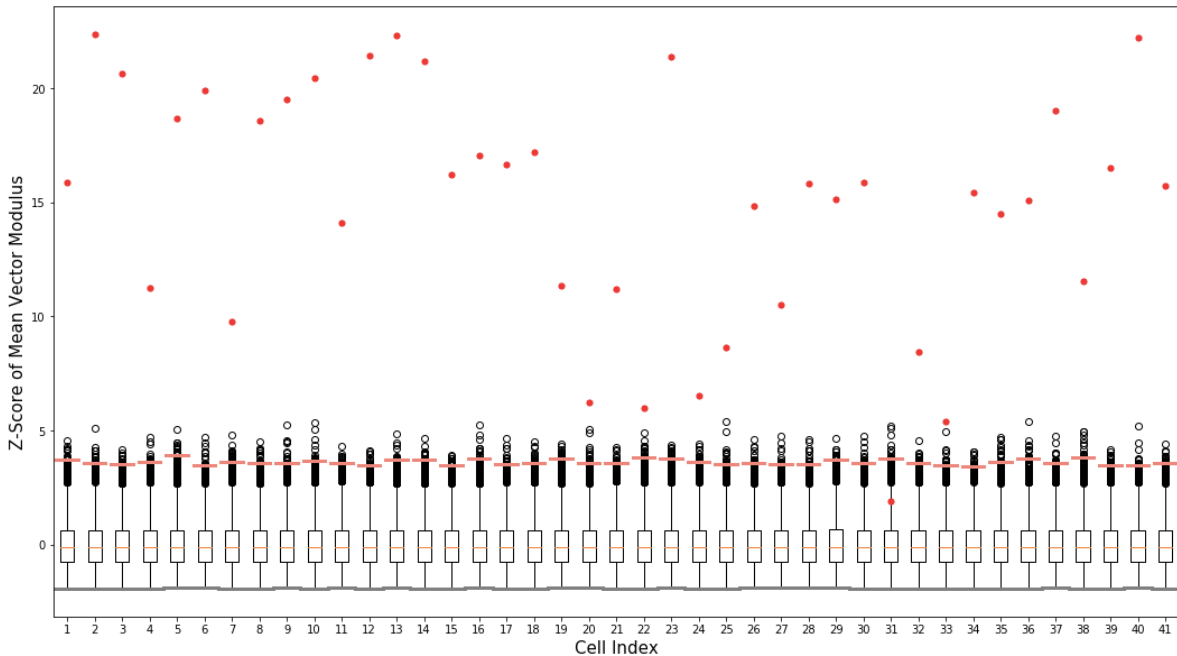


Figure 4: Z-score comparison of mean vector magnitude. Boxplot shows the distribution of the mean vector magnitude if the cell firing rate does not dependent on head angle (box extends from the lower to upper quartile values, orange line indicates median), acquired through permutation testing (10,000 permutations per cell). The pink bar indicates the

significance cut-off for each cell (Bonferroni corrected, group $\alpha = 0.05$, $m = 41$), computed non-parametrically for each cell (via directly taking the percentile value of the permutation-generated null distribution). The red dot shows the observed mean vector magnitude from the actual data. The grey line is the z-score of a vector having modulus 0 (lower bound z-score, as the vectors cannot have negative modulus).

Sec.2: Few HD fields provide better prediction of firing rates versus a uniformly distributed field

In order to assess the predictive ability of the head direction field, cross-validation is performed on each of the clusters. Concretely, for each cell, the HD field is computed from a range of *training set* data then tested on a separate *cross-validation set* composing of spikes and head directions over a different time range. Specifically, 82 cross-validations sets are selected along a “sliding-window” whereas the training sets compose of the rest of the data (Fig.5).

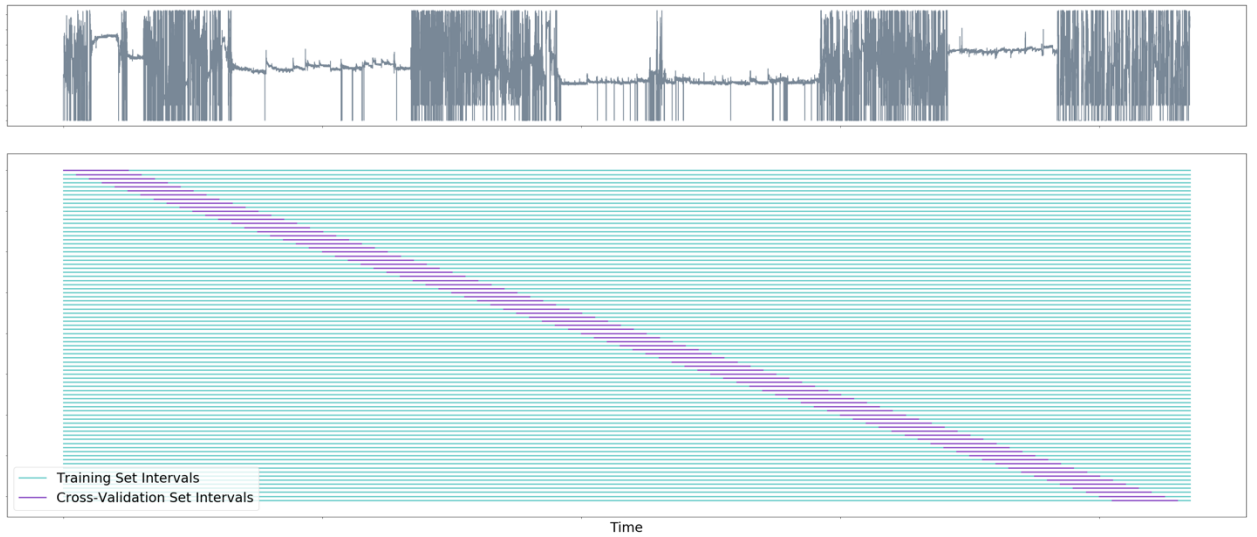


Figure 5: Visualization of the selection of the training and cross-validation sets. **Top Figure** shows the (pre-quality control) head direction of the mouse over the course of the entire recording session (just over 6 hours) for purely illustrative purposes. **Bottom Figure** shows the cross-validation and training sets, where each row represents a separate training - cross-validation trial. The cross-validation sets (purple lines), each being approximately 21 minutes of recording time (50,000 video frames), are selected at regular intervals of ~4 minutes (10,000 video frames). The training set (turquoise lines) composes of the entire recording session (870,000 video frames) excluding the section selected for cross-validation.

I chose the quadratic valuation (Q) score as a measure of prediction quality [6]. The Q-score is chosen over the log-likelihood valuation due to its robustness towards low prediction values (i.e. does not result in negative infinities when taking log 0), and because the two

measures showed no noticeable differences in trend from a preliminary analysis (not shown here). The Q-score is defined as:

$$Q = \sum_{i \in S} \lambda(t_i) - \frac{1}{2} \int \lambda(t)^2 dt$$

... where S is the set of all spiking events, and $\lambda(t)$ is the predicted firing rate at time t .

Intuitively, it rewards high predicted firing rate when there are spiking events ($\lambda(t_i)$) and penalizes high predicted firing rate when there are no spike events (via subtracting the integral of the predicted firing rate function). The higher the Q-score is, the better the predictive model performs.

Since the firing rate prediction are computed in discrete-space (i.e. per frame of video recording of the cross-validation set), the above can be approximated as:

$$Q = \sum_{i \in S} \lambda(t_i) - \frac{1}{2} \sum \lambda(t)^2 \cdot t_{window}$$

... where t_{window} is the width of a single prediction window (i.e. frame-length of video).

Since Q is a relative measure, I compared my predictive model (i.e. *HD field* for a given cell, Fig.6A) against a “null” model having an uniformly distributed firing rate across all head angles (Henceforth referred to as *uniform field*, Fig.6B). Intuitively, the uniform field “predicts” that the firing rate at each time-point is simply the average firing rate across the entire training set.

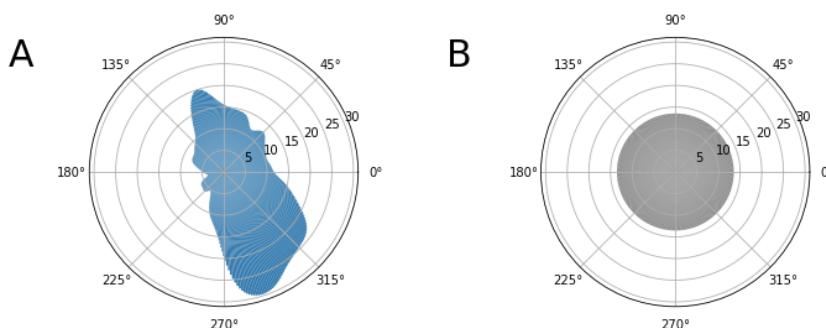


Figure 6: (A) The HD field of an illustrative cell (cluster 34), as illustrated in Fig.3. As a reminder, the HD field shows the expected average firing rate of a cell (spikes/s) given the head direction of the animal. (B) The uniform field, where the expected firing rate of the cell is constant in all directions. This constant is taken as the average firing rate of the same training set used to compute the HD field.

The Q scores for each cross-validation sets are computed (Fig.7). For instance, this cell (index 34) has a HD field that consistently performs better than the uniform field. Concretely, this means that the HD field (Fig.6A) is able to predict the activity of the cell better than that of a uniformly distributed field (Fig.6B).

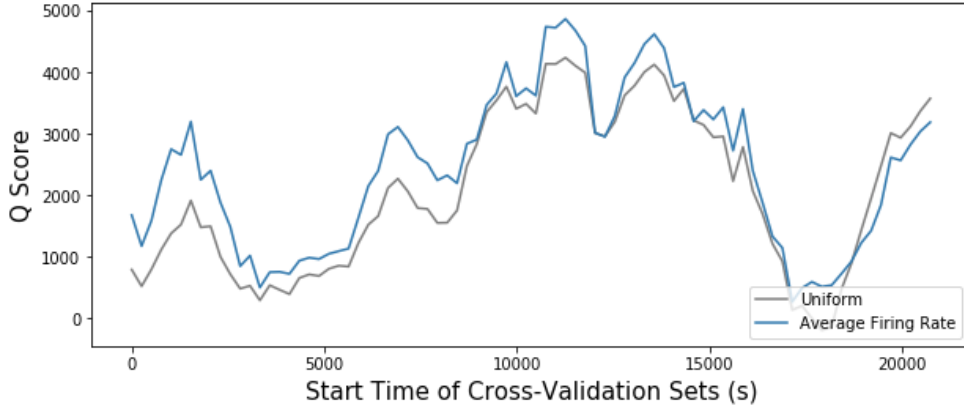


Figure 7: Q scores of the HD field compared against the Q scores of the uniform field. The horizontal axis shows the start time of each of the cross-validation sets (with reference to Fig.5, recall that the cross-validation set is taken on a “sliding window” across time).

To quantify how much better the HD field performs over the uniform field, I took the averaged difference between the two:

$$\overline{\Delta Q}_{test} = \frac{1}{n} \sum_{i=1}^n Q_{HD,i} - Q_{uniform,i}$$

... where n is the number of cross-validation sets ($n = 82$) and $\overline{\Delta Q}_{test}$ represents the averaged *improvement* in prediction quality of the HD field over the uniform field.

$\overline{\Delta Q}_{test}$ is tested against a permuted null distribution, $\overline{\Delta Q}_{null}$, acquired through randomly swapping values of $Q_{HD,i}$ and $Q_{uniform,i}$, before re-computing the averaged difference. Specifically, I generated Bernoulli trials with $p = 0.5$ for each $i = 0, \dots, n$, and swapped values if the trial returned “1”. $\overline{\Delta Q}_{null}$ shows the distribution of $\overline{\Delta Q}$ if it does not depend on the prediction model (i.e. HD vs. uniform) used, and we would therefore expect $E[\overline{\Delta Q}_{null}] = 0$.

A Bonferroni-corrected test with group $\alpha = 0.05$ is used again to compare $\overline{\Delta Q}_{test}$ with the $\overline{\Delta Q}_{null}$ distribution. Out of the 41 clusters (Fig.8), 13 (32%) have HD fields that predict cross-validation firing rates significantly better than a uniform field, as shown by significant rejection of the null hypothesis in favour of $\overline{\Delta Q}_{test} > 0$.

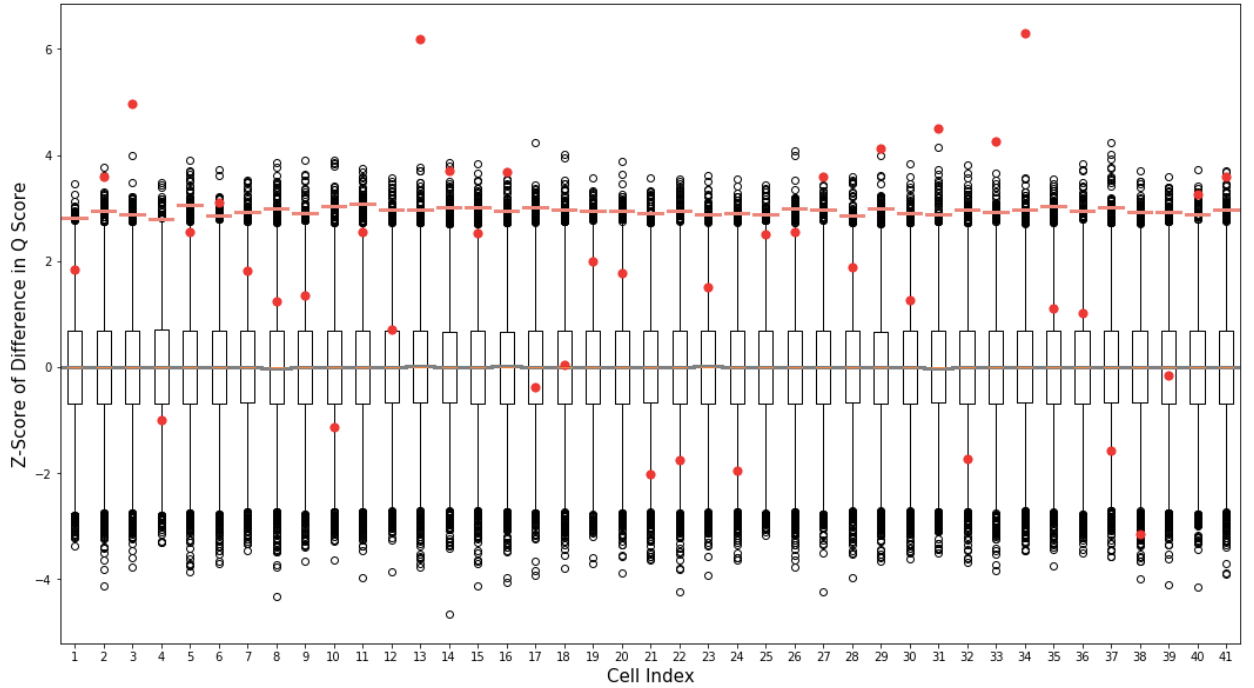


Figure 8: Z-scores of $\overline{\Delta Q}$'s. Boxplot shows the null distribution ($\overline{\Delta Q}_{null}$) as acquired by permutation testing (20,000 permutations per cluster), which indicates the distribution if the difference in Q score does not depend on the predictive field used (box extends from the lower to upper quartile values, line indicates median). The pink bar shows the significance cut-off, computed non-parametrically for each null distribution with a Bonferroni-corrected group $\alpha = 0.05$, $m = 41$. The red dot shows the $\overline{\Delta Q}_{test}$ of each cell. The grey bar shows the z-score of $\overline{\Delta Q} = 0$, which provides a good sanity check to see that the generated null distributions are all centred around 0.

Finally, the results of the above test are visualized on the HD fields of each cell (Fig.9), where the z-score for each cell is shown via a blue-red colour-map. Blue corresponds to negative z-scores, and red to positive ones (i.e. Fig.3 with color corresponding to z-scores in Fig.8). Cells that are dark red meet the significance cut-off as I have defined above.

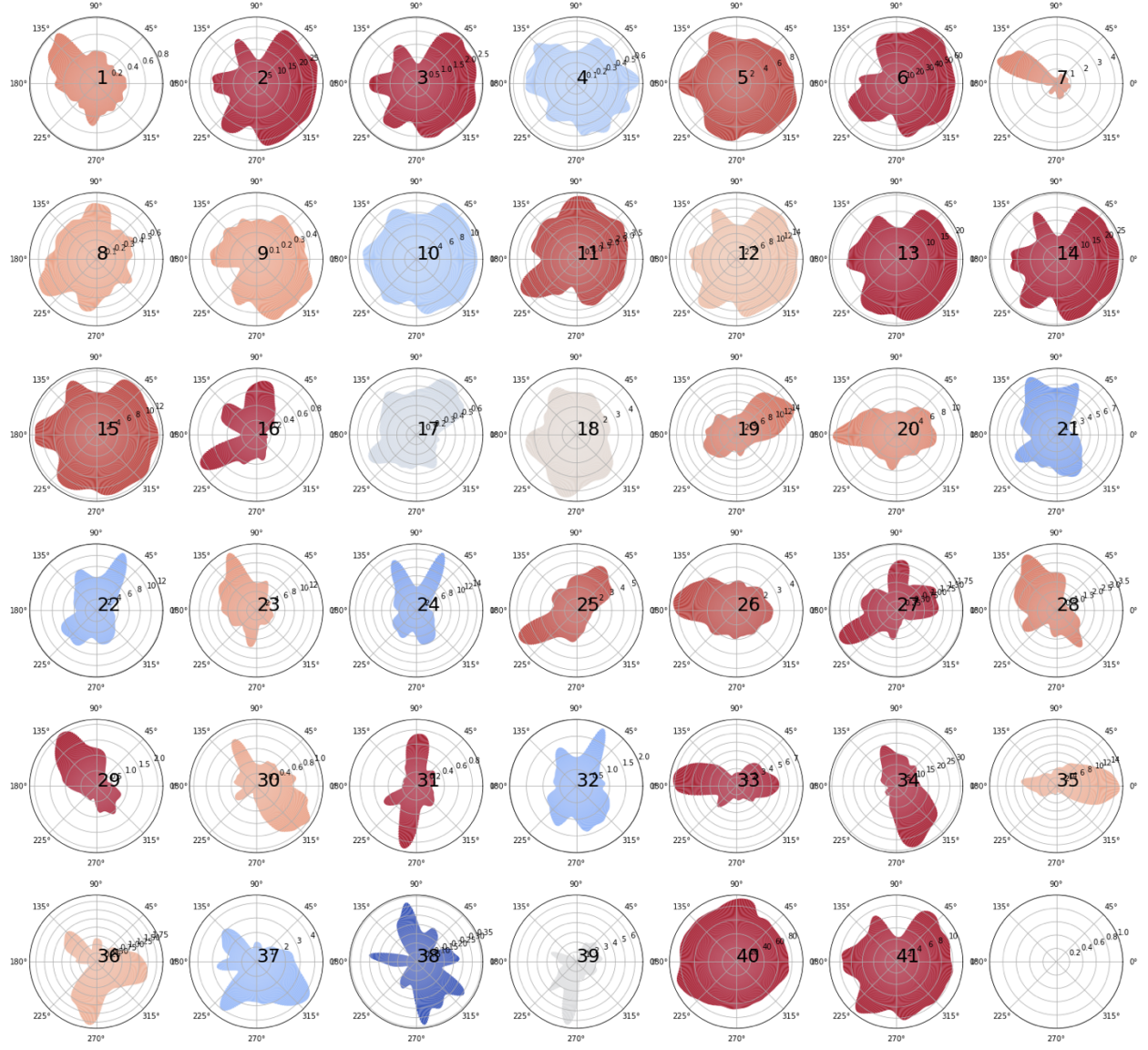


Figure 9: Each cell's HD field visualized on a polar axis, where the colour of the HD field represents the z-score of the ΔQ_{test} for that cell. A blue-red gradient is used, where blue corresponds to negative z-scores, and red to positive z-scores. All the clusters with dark, solid red meet the significance cut-off I previously defined (Bonferroni corrected with group $\alpha = 0.05$).

Discussion

The results suggest that the traditional method of evaluating head direction by the quotient of firing events over time does not always provide a good evaluation of the true, underlying directional selectivity of the neuron. Evident in the results of my confirmatory analysis, 98% of cells show significant directional dependency when testing the HD field alone, as opposed to the 32% when testing the accuracy of predicting a previously unseen spike train (tested with the same alpha level and multiple-comparison correction). Therefore, when viewed holistically, my hypothesis is supported.

Specifically, with reference to Fig.9, I observe that certain cells with highly oriented firing patterns show good predictive abilities (E.g. index 29, 33), and other cells with spread-out firing patterns show poor predictive abilities (E.g. index 4, 10). This conforms to the traditional view of HD cells. However, this is not always the case. For instance, cell index 39 shows a highly oriented firing pattern (Fig.9), yet does not exhibit good predictive abilities. In fact, index 39 predicts future spike trains much worse than cell index 13, which has a much more “spread-out” HD field. This further speak to the weakness of identifying HD cell purely by dividing total number of spikes in each direction by total time in each direction.

It is interesting to postulate on the reasoning behind the discrepancies between the HD field’s shape and its predictive abilities. For instance, it may be that a neuron undergoes burst firing under very context-specific conditions (e.g. a prior condition in addition to the animal facing south; that is to say, the cell only fires when the animal faces south but not every time it faces south). Given this is the case, the current way of computing HD field would label this neuron as a “south-sensitive HD cell”, when in fact it would be a poor encoder of the animal’s HD since it does not fire unless additional conditions are met. A potential next-step will be to look at the firing rate of neurons *each time* the animal faces a certain direction and define HD cells as cells that *consistently* fire each time the animal faces that particular direction.

A weakness in my own methodology is the permutation test for independence between head angle and firing rates (*sec. I*). Evident by Fig.9, cells with very un-concentrated HD fields and poor predictive abilities (index 4, 10) are being labelled as significant in *sec. I*. In fact, the only cell *not* labelled as significant in *sec. I* is index 31, which exhibit strong bi-directionality.

The error mainly stems from the test statistic being just the mean vector magnitude of the HD field, which has no notion of the concentration of its firing rate vectors. In the future, a test that would account for the concentration of firing rates (e.g. *Rayleigh test of non-uniformity*) may better address this issue and should also be compared against a cross-validation method as a next step analysis.

A final note is the significance level for the evaluation of prediction quality (*sec.2*). While I used the Bonferroni correction to set the significance cut-off (Fig.8, pink bars), it is used purely for consistency with *sec.1*. The Bonferroni correction may be too stringent and result in more false negatives. For the sake of HD cell discovery, an un-corrected test or the false-discovery method of correction may be more suitable, especially since the HD cell identification is often an exploratory step for other type of analysis. Likewise, as discussed above, the definition of HD cells and the process of HD cell identification should be critically evaluated prior to each experiment, as the firing rate vectors only provide a limited view of the highly complex neural code.

References

- [1] Taube JS. The head direction signal: origins and sensory-motor integration. *Annu Rev Neurosci.* 2007;30:181-207.
- [2] Taube JS. Head direction cells recorded in the anterior thalamic nuclei of freely moving rats. *J Neurosci.* 1995;15(1 Pt 1):70-86.
- [3] Rubin A, Yartsev MM, Ulanovsky N. Encoding of head direction by hippocampal place cells in bats. *J Neurosci.* 2014;34(3):1067-80.
- [4] Peyrache, A., Buzsáki, G. (2015). Extracellular recordings from multi-site silicon probes in the anterior thalamus and subicular formation of freely moving mice. CRCNS.org.
<http://dx.doi.org/10.6080/K0G15XS1>
- [5] Peyrache A, Lacroix MM, Petersen PC, Buzsáki G. Internally organized mechanisms of the head direction sense. *Nat Neurosci.* 2015;18(4):569-75.
- [6] Itskov V, Curto C, Harris KD. Valuations for spike train prediction. *Neural Comput.* 2008;20(3):644-67.

Appendix A: Simulation and Comparison of Smoothing Methods

Over the course of the analysis, various issues and bugs were encountered, with a significant one being an integer-float conversion issue that led to erroneous smoothing of histograms (specifically, the python package, *scipy*, does not properly smooth *int* variables types and the histograms should be converted to *float* before smoothing). While this bug was eventually fixed, a significant portion of the project time became dedicated to the evaluation to the smoothing methods. Since the end result became rather trivial after the bug was fixed, I decided to include this in the appendix section as the validation methodologies was still interesting to me and may provide a guide to evaluating general electrophysiological techniques.

Concretely, I simulated data in order to answer the question: when computing firing rates, is it better to smooth before dividing (the number of spiking events by the occupancy time), or divide first before smoothing?

Smoothing histograms before dividing offers better reconstruction

I generated a “ground-truth” underlying expected firing rate to head direction as a *von Mises* distribution scaled by a constant, with $\theta_0 = \pi$, $\kappa = 1$ and $C = 4$ (Fig.10):

$$f(\theta|\theta_0, \kappa) = C \cdot \frac{\exp[\kappa \cos(\theta - \theta_0)]}{2 \pi I_0(\kappa)}$$

... where $I_0(\kappa)$ is the modified Bessel function of order 0.

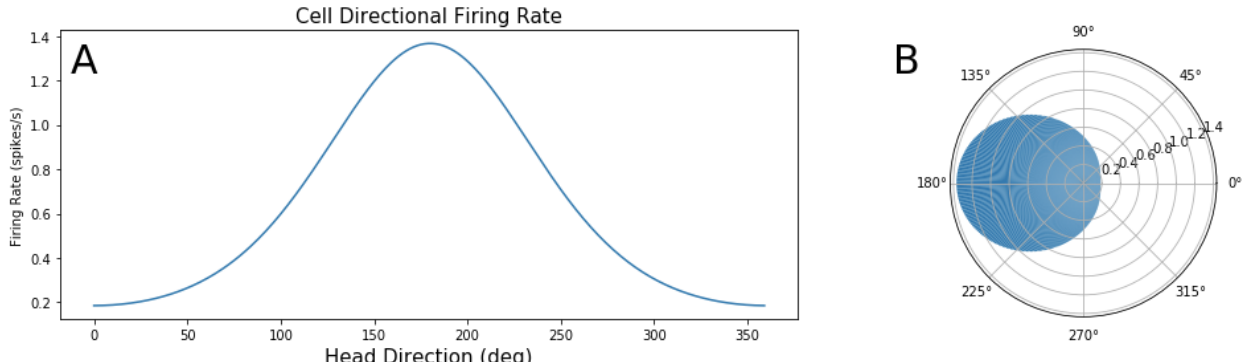


Figure 10: (A) The firing rate of this simulated directional-sensitive neuron. The firing rate is constructed by a von Mises probability density function centered at π and with $\kappa = 1$, scaled by a factor of 4 (B) The same directional sensitive firing rate as (A), plotted on a polar axis.

The head direction over the course of the “recording session” is simulated as a Gaussian walk (Fig.11A), where the head direction at each point (θ_t) is generated as:

$$\theta_t \sim \mathcal{N}(\theta_{t-1}, 1^2)$$

Having obtained the head angles, the number of spikes for each time point is modelled as an nonhomogeneous Poisson process:

$$x_t \sim \text{Poisson}(f(\theta_t))$$

...where x_t is the number of spikes at time t , and $f(\theta_t)$ is the expected firing rate given θ_t . The number of simulated spikes at each time point is drawn in Fig.11B.

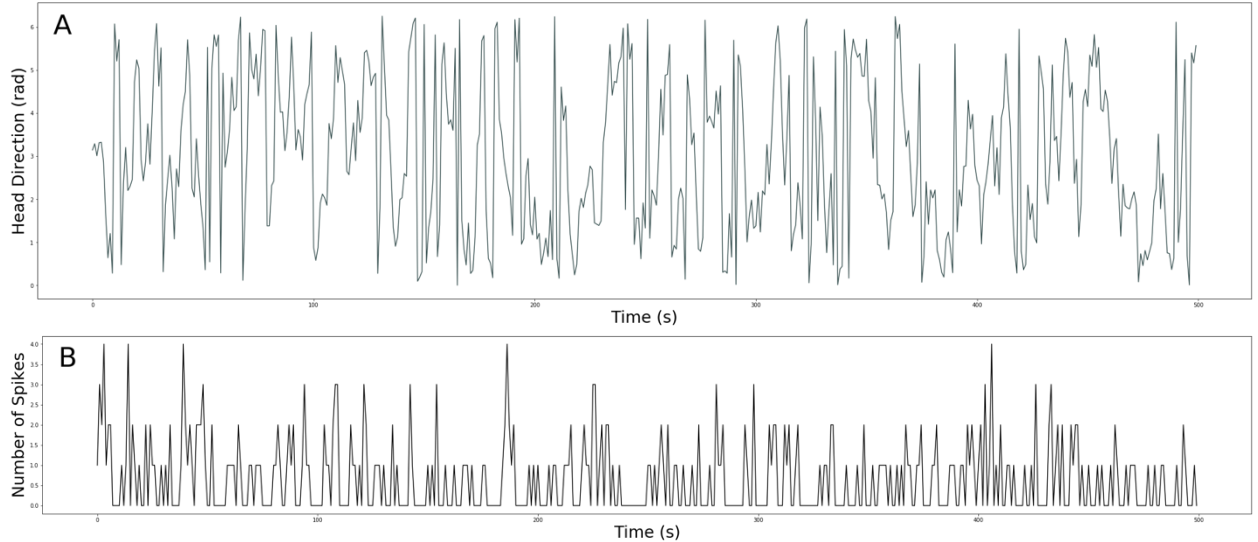


Figure 11: (A) Simulated head direction over time. Starting at $\theta = \pi$, each subsequent head direction angle is sampled from a Gaussian distribution with a standard deviation of 1 rad and mean equal to the head angle of the previous time-point. A modulus operation of 2π is taken over the entire time-series to bound the angles between 0 and 2π . (B) Simulated number of spikes at each time-point, generated as a nonhomogeneous Poisson process where the expected value at each time-point is the expected firing rate modelled by a von Mises function (Fig.10B) given the head angle at the current time-point.

From the simulated head angles and spike events, I re-constructed average firing in the same manner as before (see *Exploratory Analysis*). The only difference is I computed the average rate in two different ways: (1) By smoothing the spike and occupancy histograms first, then dividing the two (Fig.12A); (2) by dividing the spiking and occupancy histograms, then smoothing (Fig.12B).

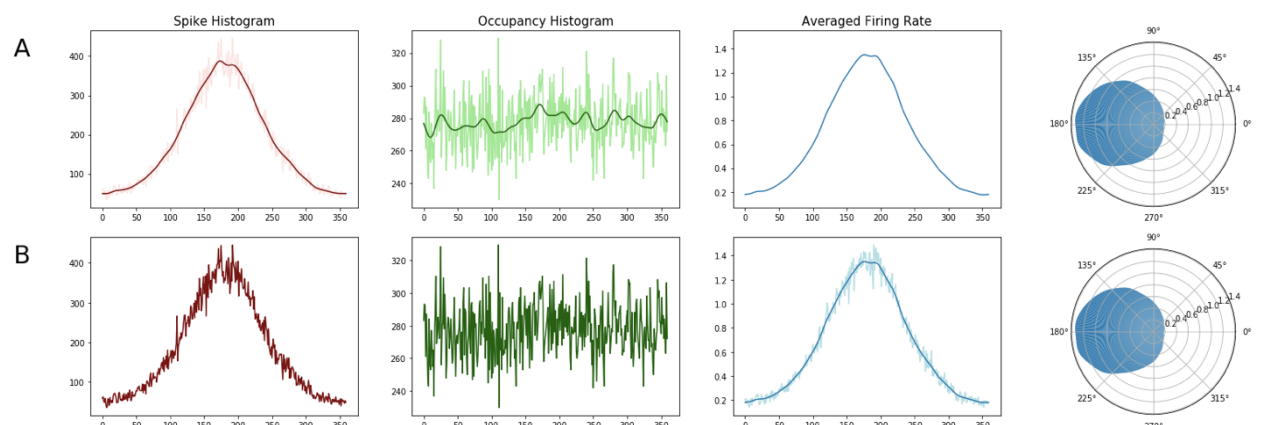


Figure 12: The steps to re-construct the average firing rate for each angle. When both light and dark colours appear in the same graph, the lighter colour is the pre-smoothed data while the darker colour is the post-smoothed data. (A) Shows the smooth-then-divide methodology of reconstructing the average firing rate field, whereas (B) Divided the spiking histogram by the occupancy histogram first before smoothing the quotient.

Evidently, the two ways of smoothing provide very similar results. When plotted against the true underlying firing rate, any difference between the two approaches is not noticeable by eye (Fig.13).

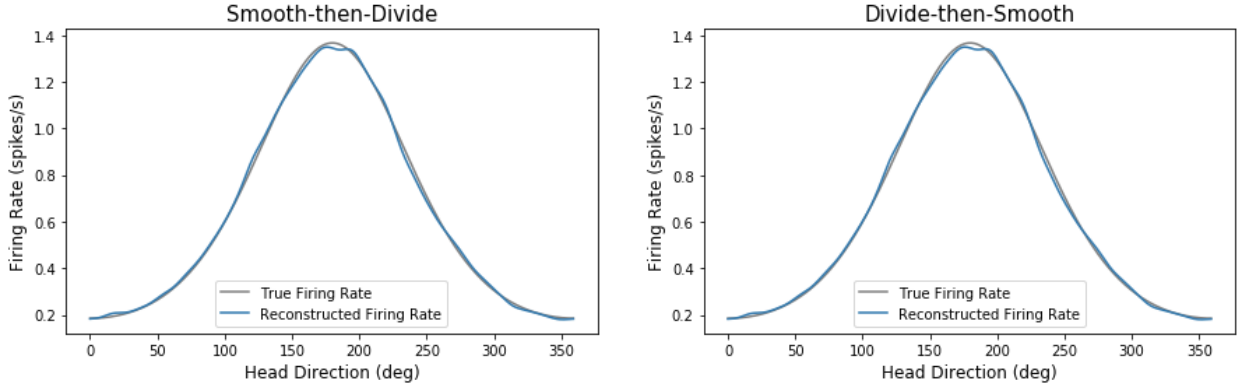


Figure 13: The reconstructed firing rate compared against the true firing rate for both the “smooth-then-divide” method and “divide-then-smooth” method.

The quality of the reconstruction is quantified via taking the squared difference between the true and reconstructed firing rate, summed over all head angles:

$$\epsilon = \sum_{\theta} (\lambda_{reconstructed}(\theta) - \lambda_{true}(\theta))^2$$

... where $\lambda(\theta)$ is the firing rate given head angle θ , and ϵ is the sum of squared error for the reconstruction.

I tested the ϵ of the two methods by repeatedly generating nonhomogeneous Poisson processes using the head angles in Fig.11A, reconstructing the head direction field and re-computing the sum of squared errors. A total of 1000 samples are simulated to generate two distributions of sum of squared errors for the “smooth-then-divide” and “divide-then-smooth” methodologies. The mean of the two distributions are compared via permutation testing (randomly shuffle elements between the two distributions and re-compute the mean difference to generate the null distribution of mean difference values). While the difference in mean, unsurprisingly, is very little, the “divide-then-smooth” reconstruction does shows significantly higher sum of squared errors to the true firing rate as compared with the “smooth-then-divide” method (Fig.14). Thus, the “smooth-then-divide” (Fig.11A) method provides better reconstruction of the true firing rate preference.

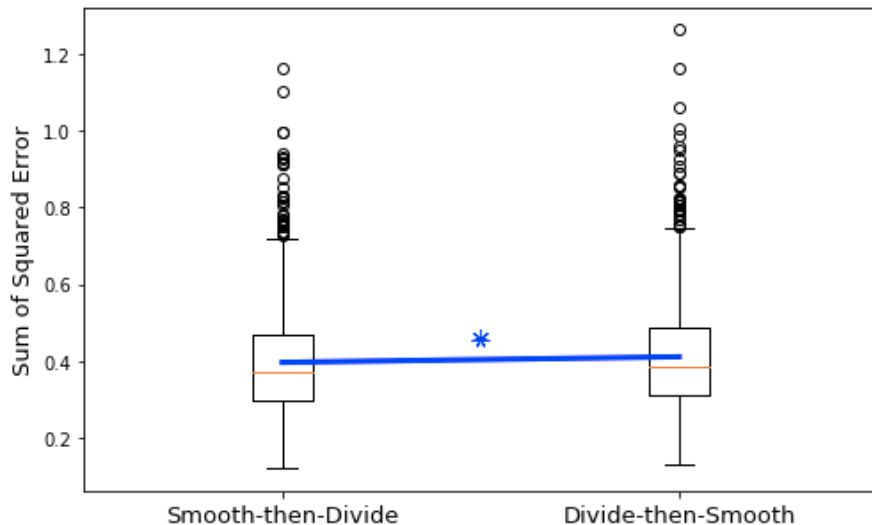


Figure 14: Boxplot showing the distribution of the sum of squared errors for the two methodologies. Blue line connects the mean value of the two distributions, which is significantly different ($p = 0.009$) when tested by a shuffling method. The boxes extend from the lower to upper quartile values, and the orange line indicates the median.

It should be noted that this difference is rather trivial – there is essentially no difference between the two reconstructions (Fig. 12), and any additional quality provided by the “smooth-then-divide” is marginal at best. Regardless, the “smooth-then-divide” method should still be recommended due to its robustness in dealing with low values in the denominator of the division (e.g. if an occupancy bin has 0 it would result in a division of 0).

Appendix B: Python Code

The *Jupyter Notebooks* used to analyze data and produce all figures in this report can be found on GitHub (not included on paper for brevity) at:

https://github.com/im-ant/NEURM012_classProject

Script Name	Script Content
ExploratoryAnalysis_HD_field_conf irmatory.ipynb	Exploratory analysis to compute the HD fields, confirmatory analysis on just the HD field alone
Confirmatory_Cross_Validation.ipynb	Confirmatory analysis using the cross-validation method
SmoothingMethods_Comparison.ipynb	Comparison of smoothing methodologies (Appendix A)